

## **A New Boundary Condition for Device Simulation Considering Outer Components**

W.Kausel, G.Nanz, S.Selberherr, H.Poetzl

Institut für Allgemeine Elektrotechnik und Elektronik  
Dept. for CAE  
Technical University of Vienna  
Gußhausstraße 27-29, A-1040 Vienna, AUSTRIA

### **Summary**

A new boundary condition has been introduced in the form of an arbitrary linear combination of voltage and current at the contact thus including both voltage and current control as special cases. Solving an additional equation devices can be simulated with simple circuits connected to device terminals. This paper describes the numerical techniques and discusses as application example the transient behavior of a  $N^+NP^+$  power diode in comparison with that of a  $N^+IP^+$  diode.

### **Introduction**

The three semiconductor equations are solved by the two-dimensional device simulator BAMBI (Franz, 1985) using the method of finite-boxes. The program simulates devices with both, geometry and doping profile being arbitrary, under steady-state or transient conditions. For a variety of applications of a device simulator the conventional voltage controlled computation is unsuitable. The definition of the contact potential is reasonable only in the case of voltage control. The ability of solving the semiconductor equations with an arbitrary linear combination of voltage and current as boundary condition allows the program to simulate a device within a circuit environment of a current source and resistive and capacitive loads. This paper specifically focuses on the definition and the numerical treatment of a boundary condition in the form of an arbitrary linear combination of voltage and current at the contact. The presented device application illustrates the use of the model.

### **Formulation**

The analysis is based on electrostatic potential, electron and hole concentration ( $\psi, n, p$ ) presumed as unknowns. According to the drift

diffusion theory (Sze, 1981), the flow of electrons and holes in a semiconductor is described by Poisson's equation (1), the continuity equation for electrons (2), the continuity equation for holes (3) and the two current equations (4,5).

$$\Delta\psi = -\frac{q}{\epsilon}(p - n + N_D - N_A) \quad (1)$$

$$\nabla J_n = q\left(\frac{\partial n}{\partial t} + R_n\right) \quad (2)$$

$$\nabla J_p = -q\left(\frac{\partial p}{\partial t} + R_p\right) \quad (3)$$

$$J_n = qD_n\nabla n - q\mu_n\nabla\psi \quad (4)$$

$$J_p = -qD_p\nabla p - q\mu_p\nabla\psi \quad (5)$$

These five equations are numerically solved with a Dirichlet boundary condition for electrons and holes at ohmic contacts. Assuming space charge neutrality directly under the terminal the concentrations are set equal to their thermal equilibrium values. The boundary condition for the electrostatic potential reads

$$V_{term} = \psi - \psi_{bi} \quad (6)$$

$$\psi_{bi} = \pm \frac{kT}{q} \ln\left(\frac{|N_D - N_A|}{n_i}\right) \quad (7)$$

where  $\psi_{bi}$  denotes the built-in potential and  $V_{term}$  the terminal voltage. Simulating contacts with external circuits,  $V_{term}$  becomes floating increasing the number of variables to be calculated by one for each floating contact. The additional equations are given by the new mixed boundary condition (8) defining the dependence between contact voltage  $V_{term}$  and contact current  $I_{term}$ .

$$\alpha \cdot V_{term} + \beta \cdot \left(I_{term} + C \frac{dV_{term}}{dt}\right) = \gamma \quad (8)$$

This is the most general form of the boundary condition which can be handled by our method. Thus, a variety of possibilities for interpretation in mathematical as well as in electrical terms, is offered. Choosing the dimensions of  $\alpha$ ,  $\beta$  and  $\gamma$  in the correct way several different definitions of the outer circuit diagram can be given using arbitrarily a serial resistive, or a parallel conductive and serial or parallel capacitive loads. A current driven circuit shown in Fig. 1 is described by defining  $\alpha = G$ ,  $\beta = 1$ ,  $\gamma = I_{appl}$ . Using expression (8)  $C$  is interpreted as a capacity parallel to the contact (Fig. 1) yielding (9).

$$G \cdot V_{term} + I_{term} + C \frac{dV_{term}}{dt} = I_{appl} \quad (9)$$

The equivalent voltage driven circuit diagram of Fig. 2 requires the assumption  $\alpha = 1$ ,  $\beta = R$ ,  $\gamma = V_{appl}$ . Interpreting  $C$  as a capacity between voltage source and contact (8) has to be slightly modified yielding (10).

$$\alpha \cdot V_{term} + \beta \cdot \left(I_{term} - C \frac{d\left(\frac{\gamma}{\alpha} - V_{term}\right)}{dt}\right) = \gamma \quad (10)$$

With the values given above the boundary condition finally reads:

$$I_{term} = \frac{V_{appl} - V_{term}}{R} + C \frac{d(V_{appl} - V_{term})}{dt} \quad (11)$$

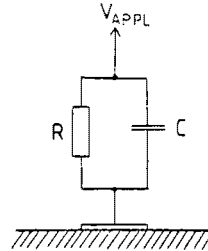
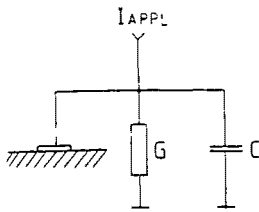


Fig.1: Equivalent circuit diagram Fig.2: Equivalent circuit diagram

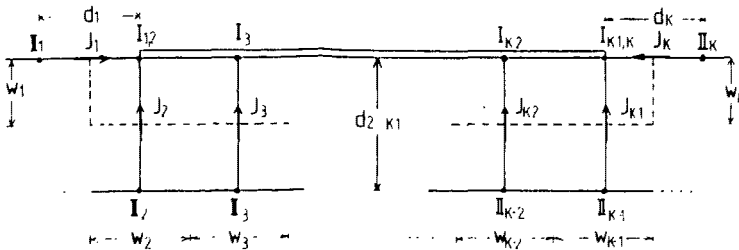


Fig.3: Section of the mesh around the contact

### Numerical Treatment

The numerical treatment of a mixed boundary conditions (8) or (10) is illustrated by Fig. 3. Both equations include the two variables  $V_{term}$  and  $I_{term}$  in which  $V_{term}$  is the additional unknown and  $I_{term}$  has to be expressed by  $\psi_i, n_i, p_i$ . The terminal current is given by integrating electron-, hole- and displacement current densities  $J_n, J_p$  and  $J_d$  over the area of the contact  $A$  (12).

$$I_{term} = \int_A (J_n + J_p + J_d) \cdot dA \quad (12)$$

Using the well known finite difference scheme first suggested by Scharfetter and Gummel (1969) the boundary conditions (8) and (10) finally yield the discrete expressions (13) and (14):

$$\alpha \cdot V_{term_T} + \beta \cdot \left( \sum_k (J_{n_k} + J_{p_k} + J_{d_k}) + C \frac{V_{term_T} - V_{term_{T-\Delta T}}}{\Delta T} \right) = \gamma \quad (13)$$

$$\alpha \cdot V_{term_T} + \beta \cdot \left( \sum_k (J_{n_k} + J_{p_k} + J_{d_k}) - C \frac{\left( \left( \frac{\partial}{\partial t} \right) T - \left( \frac{\partial}{\partial t} \right) T - \Delta T \right) - |V_{term_T} - V_{term_{T-\Delta T}}|}{\Delta T} \right) = \gamma \quad (14)$$

with

$$J_{n_k} = qD_n \frac{w_k}{d_k} [n_{II_k} B(\Delta_k) - n_{I_k} B(-\Delta_k)] \quad (15)$$

$$J_{p_k} = qD_p \frac{w_k}{d_k} [p_{I_k} B(\Delta_k) - p_{II_k} B(-\Delta_k)] \quad (16)$$

$$J_{d_k} = -\frac{w_k}{d_k} \cdot \epsilon \frac{(\psi_{II_k} - \psi_{I_k})_T - (\psi_{II_k} - \psi_{I_k})_{T-\Delta T}}{\Delta T} \quad (17)$$

$$\Delta_k = \frac{\psi_{II_k} - \psi_{I_k}}{V_t}, \quad B(x) = \frac{x}{e^x - 1} \quad (18,19)$$

where  $I$  denotes the point at the contact and  $II$  the next neighbour (Fig. 3),  $J_{n,p,d}$  denote the three current contributions at the midpoints,  $T$  the actual time,  $\Delta T$  the actual time step,  $d_k$  the distance between point  $I$  and point  $II$  and  $w_k$  the weighting factor for the integration.  $D_n$  and  $D_p$  are the coefficients for electron- and hole diffusion,  $\epsilon$  is the dielectric permittivity,  $q$  the electronic charge and  $V_t$  the thermal voltage.

The discrete form of the mixed boundary condition (13) and (14), respectively, together with a discrete representation of both continuity equations (1) and (2) and Poisson's equation (3) yield a numerical solution for electrostatic potential, electron and hole concentration  $\psi_i, n_i, p_i$  at each free node in a finite-boxes mesh (Franz, 1983; Selberherr, 1984) and the terminal voltage  $V_{term}$  for each floating contact. Since (13) and (14) are nonlinear in the unknown variable  $V_{term}$  a linearization technique is required. For current or mixed boundary problems the discretized nonlinear equation system is therefore solved simultaneously by a coupled Newton's method.

## Results of Numerical Experiments

The equations to be solved for simulating semiconductor devices which are current driven or require mixed boundary conditions form a coupled nonlinear partial integro-differential equation system. Until now no mathematical theory exists dealing with the problem of partial differential equation systems with integral boundary conditions. It is neither possible to give an a priori estimate for the solution nor even to predict solvability. Computing the solution therefore is a question of numerical experiments. However, finding a solution depends on two major factors as shown by our experience. The initial guess as well as the choice of the boundary condition in respect to the slope of the characteristic at the sought-for bias point is of considerable importance for convergence. Calculating a bias point with a high value  $g = \frac{dI}{dV}$  requires a current driven or at least an almost current driven boundary condition ( $\alpha \rightarrow 0, \beta \rightarrow 1$ ). In that case a solution might be achieved rather quickly while voltage control completely failed convergence. In other words any low current simulation with a current driven contact requires an initial guess very close to the solution. Otherwise it will be almost impossible to succeed. A voltage controlled simulation close to the requested bias point would be the best way to find a good start solution for the given problem. Nevertheless, in many cases it will be impossible to predict a bias point

for that purpose. Thus, a universal simulation program must be able to handle such difficulties by itself. We decided to use the values  $\frac{\beta}{\alpha}$  rescaled to a resistance  $R$  and  $\frac{\gamma}{\alpha}$  rescaled to a voltage  $V_{appl}$  for the initial guess of the contact voltage  $V_{term}$ . Assuming a higher voltage drop at the resistor for increased  $R$ ,  $V_{term}$  is computed by (20).

$$R \leq 10k\Omega : V_{term} = \frac{V_{appl}}{2} \quad R > 10k\Omega : V_{term} = \frac{V_{appl}}{\log_{10}(R) - 2} \quad (20)$$

The start values of all other unknowns are found assuming charge neutrality in connection with the equilibrium condition (Franz, 1985).

### Application

One major application of such a tool is the realistic simulation of the transient device behavior. To prove the capability of that implementation this paper presents the results of our investigations comparing the switching behavior of two power diodes in contrast to earlier publications dealing with short switching diodes (De Mari, 1968). The simulated devices are a  $110\mu m$  long  $N^+NP^+$  diode with a cross-section of  $100\mu m \times 100\mu m$  and a  $N^+IP^+$  diode of the same dimensions. The doping for both devices is shown in Fig. 4. The diodes were switched from  $-10V$  reverse bias at the anode to  $+10V$  taking a serial resistance into consideration.

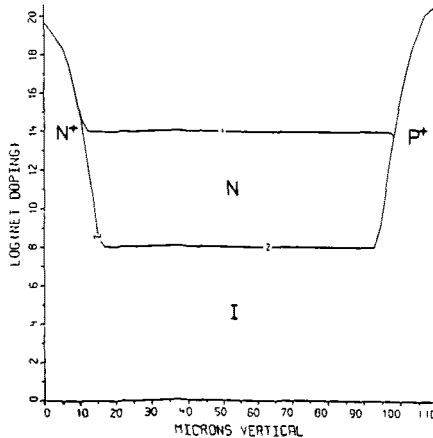


Fig.4: Doping profiles  
( $N^+NP^+$  diode and  $N^+IP^+$  diode)

Choosing a serial resistor of  $100k\Omega$  for the first simulation of the  $N^+NP^+$  diode the device reaches a final bias point of  $V_a = 0.689V$  (table 1) corresponding to a low injection state. The contact voltage (Fig. 5) shows the well known exponential behavior with a turn on time of about  $15ns$ . With a junction capacity of  $C = 69.1fF$  and a bulk resistance of  $R = 5k\Omega$  the time constant  $\tau_1$  is given by  $\tau_1 = 7.26ns$ . This very nicely fits to the initial slope of the  $V-t$  curve.

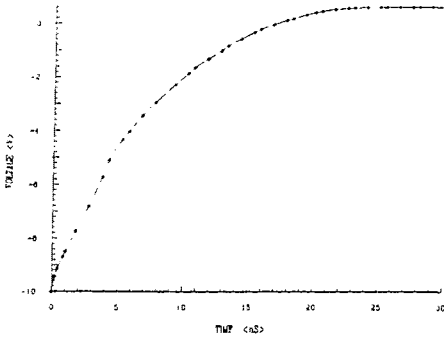


Fig. 5: V-t curve of  $N^+NP^+$  diode with  $R = 100k\Omega$

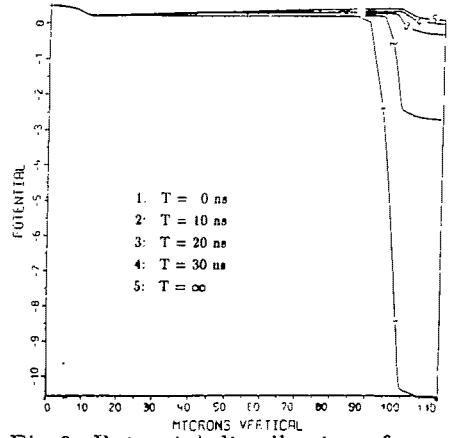


Fig. 6: Potential distribution of  $N^+NP^+$  diode with  $R = 100k\Omega$

Inspecting the distribution of electrostatic potential (Fig. 6), electron (Fig. 7) and hole concentration (Fig. 8) we see how the space charge region at the  $N^+P$  junction is decreased causing reduced voltage drop (curve 1,2). After  $20ns$  the space charge region has almost vanished (curve 3) and, since the diode is already forward biased, the anode starts to inject holes into the drift region. The steady state condition (curve 5) shows the device in a low injection state with a still existing but small space charge region (Fig. 6,7) and an exponential decay of minorities within the drift region.

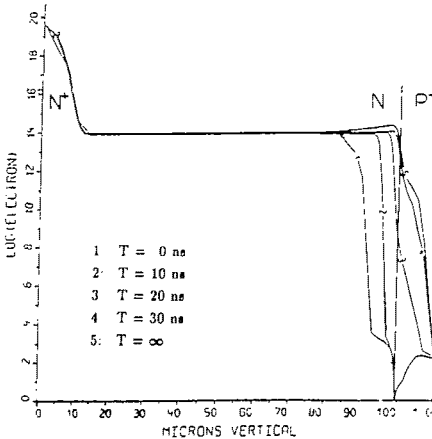


Fig. 7: Electron distribution of  $N^+NP^+$  diode with  $R = 100k\Omega$

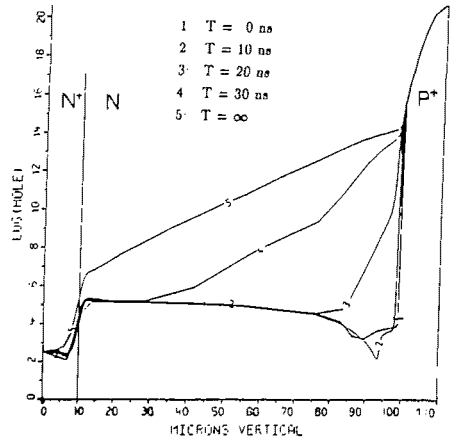


Fig. 8: Hole distribution of  $N^+NP^+$  diode with  $R = 100k\Omega$

If the external resistor  $R$  is reduced to  $1k\Omega$  it is already smaller than the bulk resistance of about  $R_B = 5k\Omega$ . Thus, the switching behavior differs completely. The figures of the anode voltage (Fig. 9) and that of the current (Fig. 10) show a capacitive behavior in the beginning with a time constant of about  $\tau_2 = 420ps$  due to the junction capacity of about  $C = 69.1fF$  and the resistance of  $R + R_B = 6k\Omega$ .

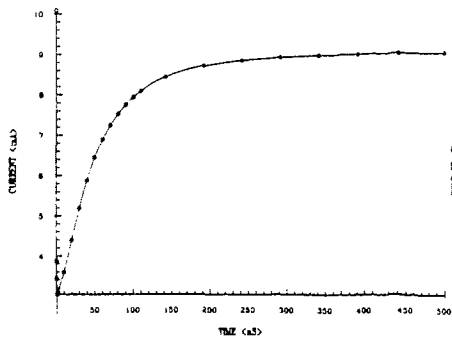


Fig.9: V-t curve of  $N^+NP^+$  diode with  $R = 1k\Omega$

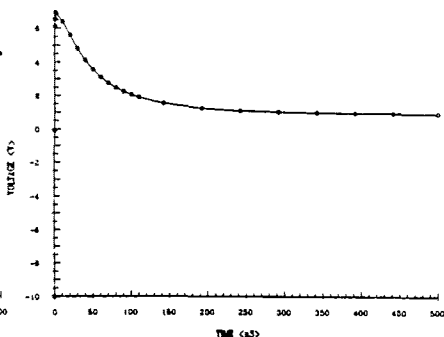


Fig.10: I-t curve of  $N^+NP^+$  diode with  $R = 1k\Omega$

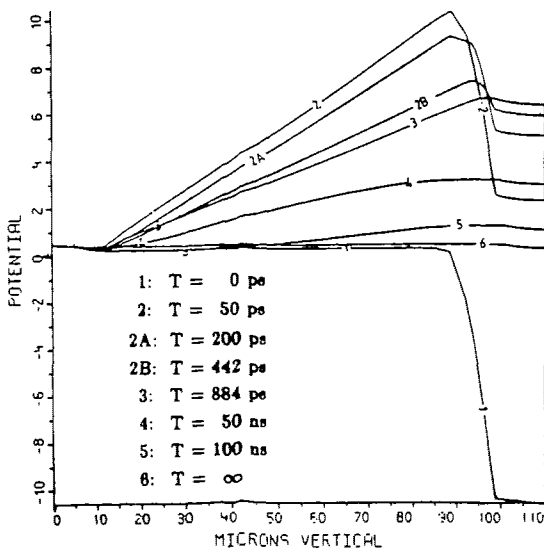


Fig.11: Potential distribution of  $N^+NP^+$  diode with  $R = 1k\Omega$

Passing the junction as displacement current the flow continues as particle current within the drift and the contact regions giving rise to a high ohmic voltage drop at the bulk resistance (Fig. 11, curve 2). Note that the device current is flowing into negative x-direction. Both carrier flows within the highly doped regions decrease with the same time constant  $\tau_2$ . However, inspecting the distribution of the potential (Fig. 11) shows a completely different behavior of the displacement current. Due to the ratio  $\frac{R_D}{R+R_D} = \frac{5}{6}$  a major part of the source voltage jump of  $\Delta V = 20V$  is transmitted to the N-doped side of the junction and shifts the potential to a value higher than  $+10V$  (Fig. 11, curve 2). This causes a dramatic increase of the field within the drift region and therefore a negative displacement current is added to the carrier current there. At that moment the electron flow within the highly doped cathode region must be smaller than that one in the drift region. The following curves show a decrease of the ohmic voltage (Fig. 11) drop due to the decrease of particle current.

This becomes apparent from particle current calculations which are not included in our figures. Thus, the displacement current changes its sign flowing into positive x-direction.

During that time of capacitive behavior the depletion region is quickly overflowed with carriers by an electron current from the drift region and a hole current from the anode region. This reduction of the depletion region reduces the positive field yielding the negative displacement current flow over the junction. So the anode potential is steadily increased (Fig. 11, curve 1-3). Reaching the anode voltage maximum of  $V_A = 7V$  (Fig. 9) corresponding to a current minimum of  $I_A = 3mA$  (Fig. 10) after about two time constants (i.e.:  $884ps$ ) the capacitive process is followed by a pseudo-inductive one. With a time constant  $\tau_3$  of about  $\tau_3 = 85ns$  90% of the final anode values are reached after about  $110ns$ . The final bias value of the anode voltage is  $V_A = 0.8513$  (table 1).

Curve 3 shows the situation at the time when the anode current reaches its minimum and the anode voltage its maximum. The device is now in a low injection state with a still existing but very small space charge region (Fig. 12). Subsequently majority and minority injection is further increased (Fig. 12,13, curve 4) consequently reducing the bulk resistance. Thus, the carrier flow increases again yielding a growing anode current. Finally the high injection state is reached which shows the same high value of  $10^{17}$  for minority and majority concentrations (Fig. 12,13; curve 5) compared to the net doping concentration of  $10^{14}$  (Fig. 4). The space charge region has completely been overflowed (Fig. 13, curve 5).

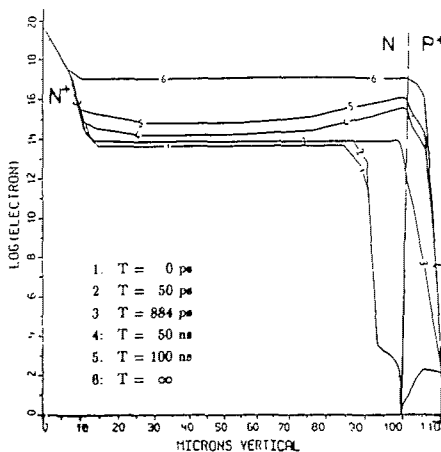


Fig.12: Electron distribution of  $N^+NP^+$  diode with  $R = 1k\Omega$

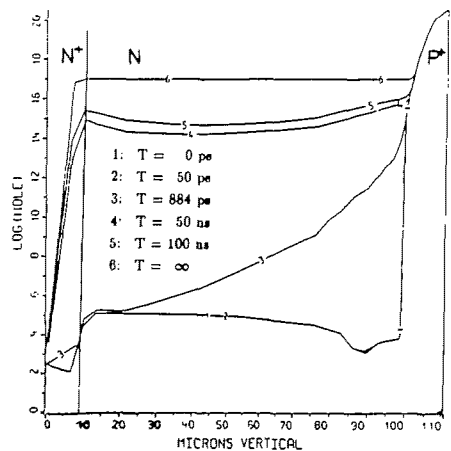


Fig.13: Hole distribution of  $N^+NP^+$  diode with  $R = 1k\Omega$

Switching a  $N^+IP^+$  diode with a  $R = 100k\Omega$  load again yields a capacitive behavior followed by a pseudo-inductive one (Fig. 14,15). With a time constant  $\tau_1$  of about  $1.2ns$  due to the capacity of the drift region of about  $C_{DR} = 11.5fF$  the high anode voltage maximum of  $V_A = 6.5V$  corresponding to the current minimum of  $35\mu A$  is reached after  $8ns$  (Fig. 14,15). 90% of the final anode values are reached after about  $75ns$ .

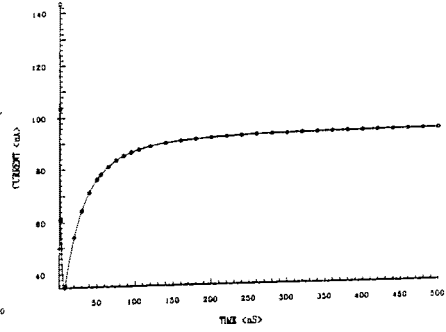
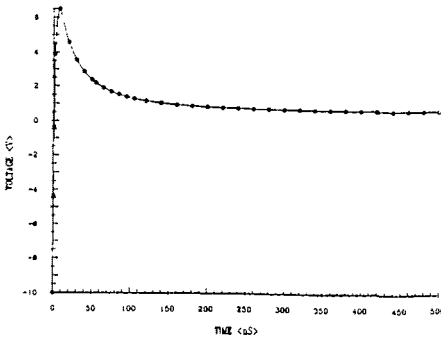


Fig.14: V-t curve of  $N^+IP^+$  diode with  $R = 100k\Omega$       Fig.15: I-t curve of  $N^+IP^+$  diode with  $R = 100k\Omega$

The undoped drift region is highly resistive to any particle current during the capacitive part of the switching. Any current must flow as displacement current within that region continuing as carrier flow of the same magnitude within the highly doped contact regions. Though the current flow through the entire device decreases with  $\tau_4$  carrier injection from both sides of the device takes place (Fig. 17,18) building up the electron-hole plasma within the drift region. This injected charge mainly defines the potential distribution (Fig. 16). The negative charge, injected from the cathode side, causes a positively bent potential, whereas the positive charge from the anode region causes a negative bend. Thus, charge injection yields the increase in electric field being necessary for the displacement current.

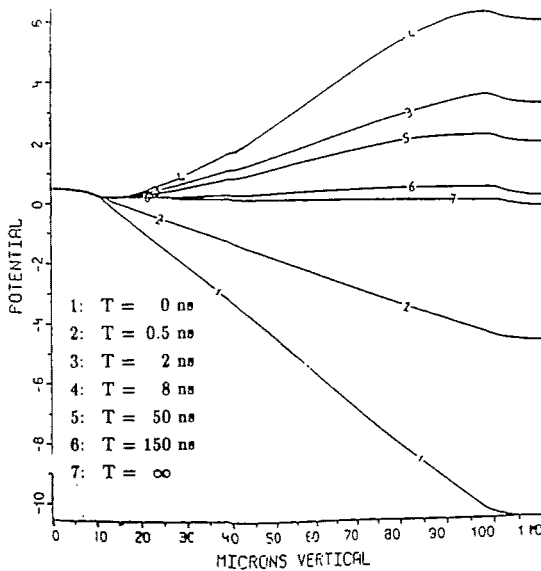


Fig.16: Potential distribution of  $N^+IP^+$  diode with  $R = 100k\Omega$

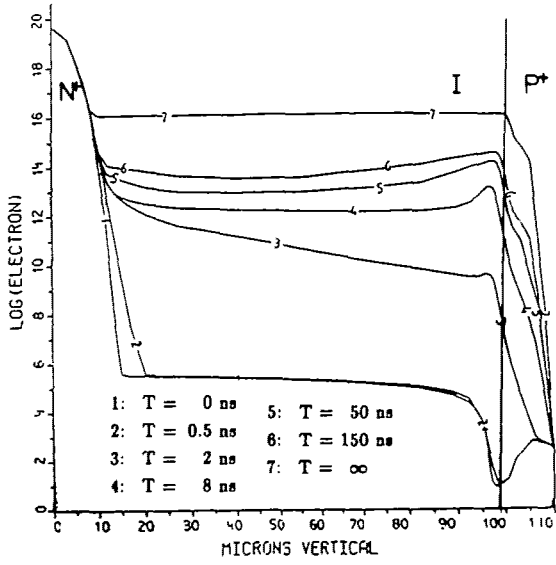


Fig.17: Electron distribution of  $N^+IP^+$  diode with  $R = 100k\Omega$

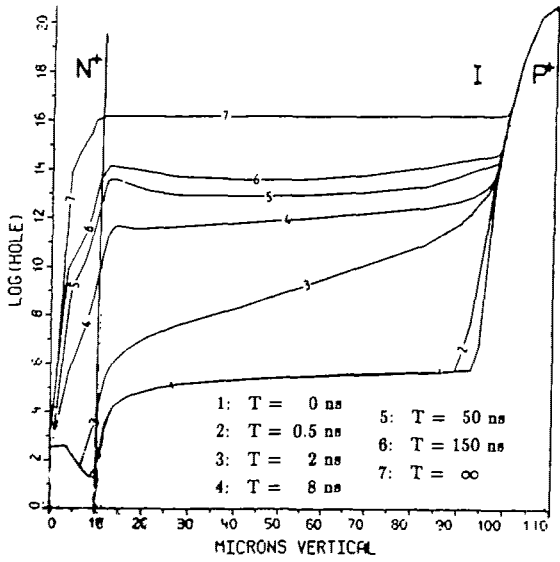


Fig.18: Hole distribution of  $N^+IP^+$  diode with  $R = 100k\Omega$

After  $8ns$  both carrier concentrations exceed the intrinsic value (Fig. 17,18, curve 4), the device comes into a high-injection state and both carrier currents flow over the entire drift region. The anode current starts to increase significantly due to the strong decrease of the bulk resistance. Since the charge is slowly neutralized on both sides of the drift region the bend in the potential distribution decreases while reducing the electric field. The displacement current therefore has changed sign and enlarges the carrier flow thus supporting the build-up of the plasma. In steady-state condition both space charge regions are completely overflowed and the electron and hole concentration show the same high value of  $10^{16}$  being constant over the entire drift region.

Table 1. Steady-state anode characteristics

Device	R	Voltage	Current
$N^+NP^+$	100 k $\Omega$	0.6891 V	93.11 $\mu A$
$N^+NP^+$	1 k $\Omega$	0.8513 V	9.149 mA
$N^+IP^+$	100 k $\Omega$	0.7047 V	92.95 $\mu A$

### Conclusion

A linear combination of terminal voltage and terminal current has been defined and successfully implemented into the BAMBI program enabling the user to consider external circuits. Numerical experiments showed a severe dependence of the convergence on the initial guess. Simulating the turn-on of a  $N^+NP^+$  diode with different contact resistors proved the dependence of the switching behavior on the final injection level. The turn on of a  $N^+IP^+$  diode showed pseudo-inductive behavior due to the high-impedance drift region.

### Acknowledgement

This work was supported by the SIEMENS AG. Research Laboratories, Munich, Germany and by DIGITAL EQUIPMENT CORP. at Hudson, U.S.A. and by the 'Fond zur Förderung der wissenschaftlichen Forschung', project S43/10. The authors would like to thank the 'Interuniversitäre Rechenzentrum' for supplying the large amount of computer resources.

## References

- Franz A. F., G. A. Franz, (1985). BAMBI-A Design Model for Power MOSFET's. *IEEE Trans. on CAD*, Vol.Cad-4, No.3, July 85, pp.177-188
- Sze S. M. (1981). Basic Equations for Semiconductor-Device Operation. In *Physics of Semiconductor Devices*, 2nd Ed., J. Wiley & Sons , USA. pp 50.
- Scharfetter D. L., H. K. Gummel, (1969). Large-Signal Analysis of a Silicon Read Diode Oscillator. *IEEE Trans. on Electr. Dev.*, Vol. ED-16 pp. 64-77.
- Franz A. F., G. A. Franz, S. Selberherr, Ch. Ringhofer, P. Markowich (1983). Finite Boxes-A Generalization of the Finite-Differences Method Suitable for Semiconductor Device Simulation. *IEEE Trans. on Electr. Dev.*, Vol. ED-30, No.9, Sept 83, pp.1070-1082
- Selberherr S. (1984). Finite Boxes. In *Analysis and Simulation of Semiconductor Devices*, Springer, New York, Vienna. pp.175-180.
- De Mari A. (1968). An Accurate Numerical One-Dimensional Solution of the P-N Junction under Arbitrary Transient Conditions. *Solid-State Electronics*, Vol. 11, pp.1021-1053.